Pramana – J. Phys. (2019) 93:12
https://doi.org/10.1007/s12043-019-1786-3

Coexistence of attractors in integer- and fractional-order three-dimensional autonomous systems with hyperbolic sine nonlinearity: Analysis, circuit design and combination synchronisation

SIFEU TAKOUGANG KINGNI[1], JUSTIN ROGER MBOUPDA PONE[2,*], GAETAN FAUTSO KUIATE[3] and VIET-THANH PHAM[4,5]

[1]Department of Mechanical, Petroleum and Gas Engineering, Faculty of Mines and Petroleum Industries, University of Maroua, P.O. Box 46, Maroua, Cameroon
[2]Department of Electrical Engineering, Fotso Victor University Institute of Technology (IUT-FV), University of Dschang, P.O. Box 134, Bandjoun, Cameroon
[3]Department of Physics, Higher Teacher Training College, University of Bamenda, P.O. Box 39, Bamenda, Cameroon
[4]Faculty of Electrical and Electronic Engineering, Phenikaa Institute for Advanced Study (PIAS), Phenikaa University, Yen Nghia, Ha Dong District, Hanoi 100000, Vietnam
[5]Phenikaa Research and Technology Institute (PRATI), A&A Green Phoenix Group, 167 Hoang Ngan, Hanoi 100000, Vietnam
*Corresponding author. E-mail: mboupdapone00@gmail.com

MS received 23 August 2018; revised 7 December 2018; accepted 13 December 2018; published online 8 May 2019

Abstract. This paper reports the results of the analytical, numerical and analogical analyses of integer- and fractional-order chaotic systems with hyperbolic sine nonlinearity (HSN). By varying a parameter, the integer order of the system displays transcritical bifurcation and new complex shapes of bistable double-scroll chaotic attractors and four-scroll chaotic attractors. The coexistence among four-scroll chaotic attractors, a pair of double-scroll chaotic attractors and a pair of point attractors is also reported for specific parameter values. Numerical results indicate that commensurate and incommensurate fractional orders of the systems display bistable double-scroll chaotic attractors, four-scroll chaotic attractors and coexisting attractors between a pair of double-scroll chaotic attractors and a pair of point attractors. Moreover, the physical existence of chaotic attractors and coexisting attractors found in the integer-order and commensurate fractional-order chaotic systems with HSN is verified using PSIM software. Numerical simulations and PSIM results have a good qualitative agreement. The results obtained in this work have not been reported previously in three-dimensional autonomous system with HSN and thus represent an enriching contribution to the understanding of the dynamics of this class of systems. Finally, combination synchronisation of such three-coupled identical commensurate fractional-order chaotic systems is analysed using the active backstepping method.

Keywords. Chaos; multiscroll attractor; bistable and coexisting attractors; fractional-order system; electronic circuit; combination synchronisation.

PACS Nos 05.40.–a; 05.40.Ac; 05.45.Pq; 05.45.Gg

1. Introduction

A major area of interest within the field of nonlinear dynamics is the investigation of systems with chaotic behaviours [1–5]. Chaotic system has been the subject of many investigations ranging from glucose–insulin regulatory system [6], homopolar disc dynamo [7], brushless DC motor [8] to Hindmarsh–Rose neuron [9] where researchers have concentrated on both integer- and fractional-order chaotic systems [10–12]. In the literature, various applications of integer- and fractional-order chaotic systems such as random bit generator, secure communications, etc. [13–17] have been reported.

There has been a growing interest in multiscroll chaotic attractor systems over the past few years. In this connection [18–22], four-scroll butterfly attractor was reported by Elwakil *et al* [18]. Qi *et al* [19] introduced a new three-dimensional quadratic autonomous system displaying a four-scroll chaotic attractor. Different approaches for constructing multiscroll attractors and grid multiscroll attractors were proposed [20–23]. Three-dimensional grid multiscroll chaotic attractors were verified by simulations and circuit experiments [24]. Recently, an interesting research was conducted by Jia *et al* [25], who analysed a four-scroll fractional-order chaotic system and implemented it for chaos-based communications. This work was carried out following the conclusions of previous research studies, establishing that the complex dynamics of systems with multiscroll attractors is more attractive than those of the conventional systems [26].

In recent years, studies on the coexistence of attractors in nonlinear systems have gained increasing attention [27–30] because they confer nonlinear systems with rich dynamics [31–33]. However, the sudden switch to undesired attractors causes some risks [27]. Although there are numerous studies related to the coexistence of attractors in integer-order chaotic systems [34–39], there has been little discussion about the coexistence of attractors in fractional-order chaotic systems with multiscroll attractors [40].

In this work, a three-dimensional autonomous system with coexisting attractors and its fractional-order form are investigated. Analyses of integer- and fractional-order autonomous systems with four-scroll attractor are presented in §2. Electronic circuit simulations are presented in §3, whereas combination synchronisation of commensurate fractional-order system with coexisting attractors is reported in §4. Section 5 gives the concluding remarks of our work.

2. Analysis of integer- and fractional-order systems with four-wing chaotic attractor

The fractional-order form of a three-dimensional autonomous system with hyperbolic sine nonlinearity introduced by Wang *et al* [41] is described by the following nonlinear differential equations:

$$\frac{\mathrm{d}^{q_1}x}{\mathrm{d}t^{q_1}} = -ax + yz, \tag{1a}$$

$$\frac{\mathrm{d}^{q_2}y}{\mathrm{d}t^{q_2}} = xz - \sinh(y), \tag{1b}$$

$$\frac{\mathrm{d}^{q_3}z}{\mathrm{d}t^{q_3}} = z - xy, \tag{1c}$$

where a is a positive real parameter. For background theory on fractional-order calculus, the readers should refer to [42–44]. System (1) is invariant under the transformation $S(x, y, z) \to (-x, -y, z)$ and has five equilibrium points: $E_0(0, 0, 0)$, $E_{1,2}(\pm\sqrt{(\sinh(\sqrt{a})/\sqrt{a})}, \sqrt{a}, \pm\sqrt{\sqrt{a}\sinh(\sqrt{a})})$ $E_{3,4}(\pm\sqrt{(\sinh(\sqrt{a})/\sqrt{a})}$ and $-\sqrt{a}, \mp\sqrt{\sqrt{a}\sinh(\sqrt{a})}$.

2.1 *Analysis of integer-order three-dimensional autonomous system with hyperbolic sine nonlinearity*

Wang *et al* [41] reported the analysis, electronic implementation and synchronisation in integer order of system (1). They demonstrated that, despite its simple structure, the integer order of system (1) displays double-scroll and four-scroll chaotic attractors and bistable limit cycles or double-scroll chaotic attractors. In this subsection, we shall show that integer order of system (1) can exhibit transcritical bifurcation, new shapes of bistable double-scroll chaotic attractors and four-scroll chaotic attractors and coexistence among four-scroll chaotic attractor, a pair of double-scroll chaotic attractors and a pair of point attractors. The characteristic equation of integer order of system (1) at the equilibrium point $E(x^*, y^*, z^*)$ is

$$\begin{aligned}&\lambda^3 + [a - 1 + \cosh(y^*)]\lambda^2\\ &\quad + [(x^*)^2 + (y^*)^2 - (z^*)^2\\ &\quad -a + (a - 1)\cosh(y^*)]\lambda\\ &\quad + 2(x^*)(y^*)(z^*) + a(x^*)^2\\ &\quad +(z^*)^2 + [(y^*)^2 - a]\cosh(y^*) = 0.\end{aligned} \tag{2}$$

For equilibrium $E_0(0, 0, 0)$, one has $\lambda^3 + a\lambda^2 - \lambda - a = 0$ and the eigenvalues are $\lambda_1 = a$, $\lambda_2 = 1$ and $\lambda_3 = -1$. Since $\lambda_1, \lambda_2 > 0$ and $\lambda_3 < 0$, E_0 is a saddle point for the integer order of system (1). In the following, consider the stability of the integer order of system (1) at the equilibrium points $E_{1,2}$ and $E_{3,4}$. Due to the invariance of system (1) under the transformation $(x, y, z) \to (-x, -y, z)$, the stability of the integer order of system (1) at the equilibrium points $E_{1,2}$ and $E_{3,4}$ can be calculated similarly. For the equilibrium point E_1, one has

$$\begin{aligned}&\lambda^3 + [a - 1 + \cosh(\sqrt{a})]\lambda^2\\ &\quad +(a - 1)\left[\frac{\sqrt{a}}{a}\sinh(\sqrt{a}) - \cosh(\sqrt{a})\right]\lambda\\ &\quad +4\sqrt{a}\sinh(\sqrt{a}) = 0.\end{aligned} \tag{3}$$

Based on Routh–Hurwitz criterion, the real parts of all the roots of eq. (3) are negative if and only if

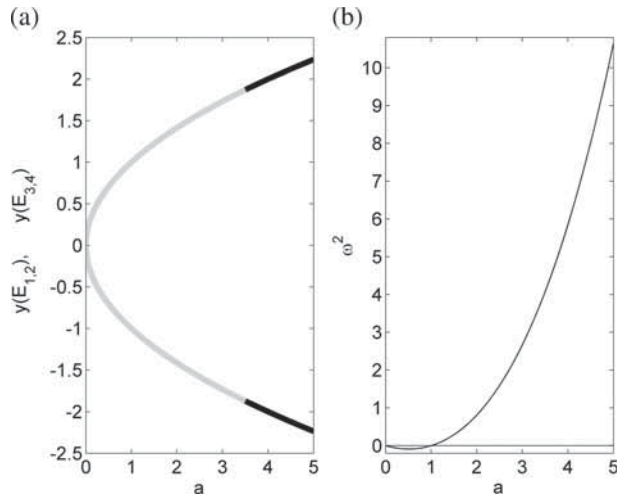

Figure 1. (**a**) Stability diagram of the equilibrium points $E_{1,2}$ and $E_{3,4}$ vs. parameter a and (**b**) the expression ω^2 (see eq. (5a)) vs. the parameter a. In (**a**), the black line indicates the stable branches and the grey line indicates the unstable branches.

$$a - 1 + \cosh(\sqrt{a}) > 0, \tag{4a}$$

$$4\sqrt{a}\sinh(\sqrt{a}) > 0, \tag{4b}$$

$$(a-1)[a - 1 + \cosh(\sqrt{a})] \times \left[\frac{\sqrt{a}}{a}\sinh(\sqrt{a}) - \cosh(\sqrt{a})\right] - 4\sqrt{a}\sinh(\sqrt{a}) > 0. \tag{4c}$$

The stability analysis of $E_{1,2}$ and $E_{3,4}$ as a function of the parameter a is shown in figure 1a.

Figure 1a shows that the equilibrium points $E_{1,2}$ and $E_{3,4}$ are unstable for $0.0001 \leq a < 3.5$ and stable for $a > 3.5$. As the equilibrium point $E_{1,2}$ or $E_{3,4}$ changes the stability properties at $a \approx 3.5$, the integer order of system (1) has either a Hopf or a transcritical bifurcation at $a \approx 3.5$. In figure 1b for $a < 1$, we get $\omega^2 < 0$, whereas for $a > 1$, we have $\omega^2 > 0$.

Theorem. *There exists no Hopf bifurcation for the integer order of system* (1) *at equilibrium point* $E_{1,2}$ *or* $E_{3,4}$ *provided* $a < 1$.

Proof. Replacing $\lambda = \mathrm{i}\omega$ into eq. (3) and separating real and imaginary parts, we obtain

$$\omega^2 = (a-1)\left[\frac{\sqrt{a}}{a}\sinh(\sqrt{a}) - \cosh(\sqrt{a})\right], \tag{5a}$$

$$(a-1)[a - 1 + \cosh(\sqrt{a})] \times \left[\frac{\sqrt{a}}{a}\sinh(\sqrt{a}) - \cosh(\sqrt{a})\right] - 4\sqrt{a}\sinh(\sqrt{a}) = 0. \tag{5b}$$

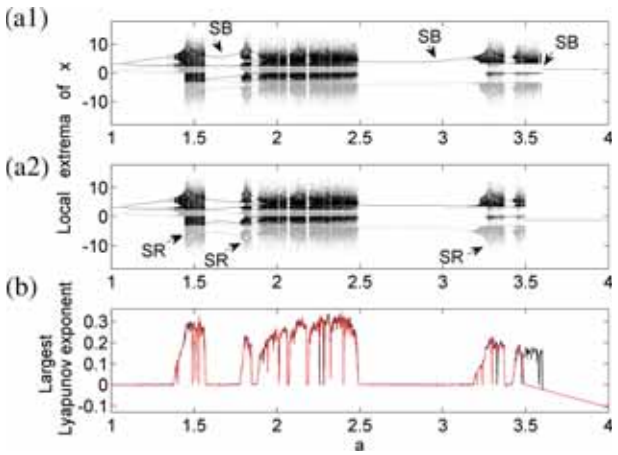

Figure 2. Bifurcation diagram depicting (**a**) the local maxima (black dots) and local minima (grey dots) of $x(t)$ and (**b**) the largest Lyapunov exponent vs. the parameter a for $q_1 = q_2 = q_3 = q = 1$. The control parameter is varied in upward direction ((**a1**) curve for the bifurcation diagram and (**a2**) curve for maximum Lyapunov exponent plot) and in downward direction ((**a2**) curve for the bifurcation diagram and red curve for the maximum Lyapunov exponent plot). The acronym SB corresponds to symmetry breaking, whereas SR corresponds to symmetry restoring.

From figure 1b for $a < 1$, we get $\omega^2 < 0$, which is not possible. Therefore, the equilibrium point $E_{1,2}$ or $E_{3,4}$ has no Hopf bifurcation. Therefore, the integer order of system (1) at equilibrium point $E_{1,2}$ or $E_{3,4}$ has a transcritical bifurcation at $a \approx 3.5$. □

Wang *et al* [41] presented the bifurcation diagram depicting the local maximum of $x(t)$ and the largest Lyapunov exponent vs. the parameter a for $1.0 \leq a \leq 2.0$ in order to find different dynamical behaviours of integer order of system (1). In figure 2, we plot the bifurcation diagram depicting the local extrema of $x(t)$ and the largest Lyapunov exponent vs. parameter a for $1.0 \leq a \leq 4.0$.

When a varies from 1.0 to 4.0 (see black dot in figure 2a1), the system exhibits period-1 oscillations followed by period-2 oscillations until the chaotic oscillations. Some periodic windows alternate with chaos for a in the range $1.09 < a < 3.598$. By further increasing the parameter a, the integer order of system (1) displays no oscillations and the trajectories of outputs $x(t)$, $y(t)$, $z(t)$ converge to the equilibrium point E_1 or E_3. When performing the same analysis by ramping the parameter a (see red dot in figure 2a2), the output $x(t)$ displays the same dynamical behaviours as in figure 2a1 in the range $1.0 \leq a < 3.5$. In the range $3.5 < a \leq 4.0$, the output $x(t)$ presents no oscillations and the trajectories of outputs $x(t)$, $y(t)$, $z(t)$ converge to the equilibrium point E_2 or E_4. By comparing

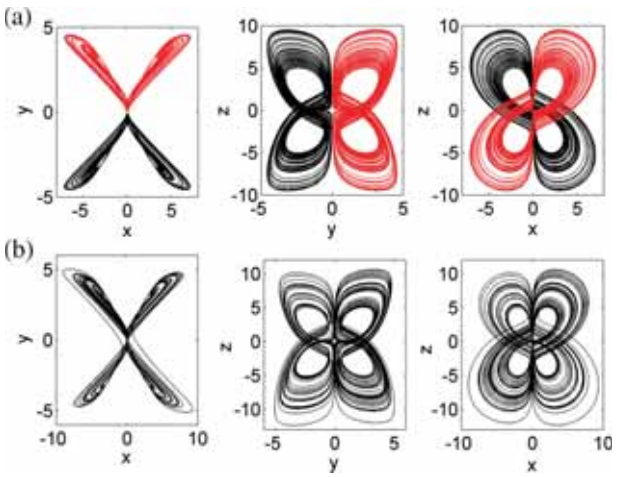

Figure 3. Phase portraits in the (x, y), (y, z) and (x, z) planes for specific value of a and initial conditions: (**a**) $a = 3.25$ and (**b**) $a = 3.35$. The curve in black is obtained by using the initial conditions $(x(0), y(0), z(0)) = (0.1, 0.1, 0.1)$, whereas curve in red is obtained by using the starting point $(x(0), y(0), z(0)) = (-0.1, -0.1, -0.1)$.

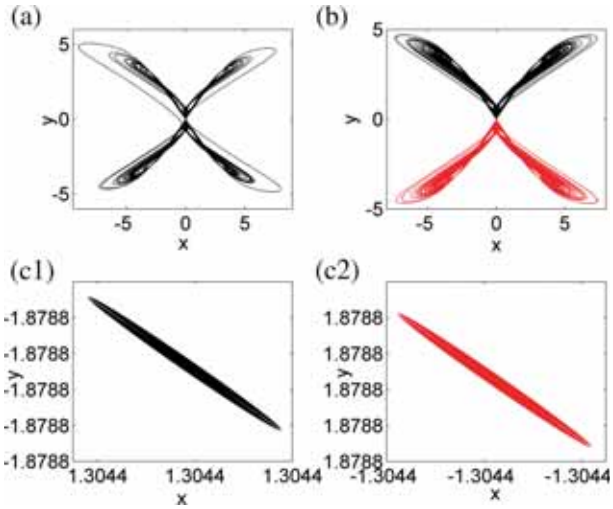

Figure 4. Phase portrait in the (x, y) plane of coexisting attractors at $a = 3.53$ and for specific values of starting points: (**a**) $(x(0), y(0), z(0)) = (0.1, 0.1, 0.1)$, (**b**) $(x(0), y(0), z(0)) = (-2, 0.1, 0.1)$ for black line and $(x(0), y(0), z(0)) = (2, -0.1, 0.1)$ for red line, (**c1**) $(x(0), y(0), z(0)) = (1.3052, -1.8788, -2.4506)$ and (**c2**) $(x(0), y(0), z(0)) = (-1.3052, 1.8788, -2.4506)$.

figures 2a1 and 2a2, one can notice that the integer order of system (1) displays the coexistence of chaotic and point attractors in the range $3.5 < a \leq 3.598$. The bifurcation diagrams in figures 2a1 and 2a2 also present the bistability phenomenon and the sequence of alternation of symmetry restoring and symmetry breaking bifurcations starting and ending by a symmetry breaking bifurcation. The largest Lyapunov exponents shown in figure 2b confirm the results found in figures 2a1 and 2a2. The chaotic behaviour shown in figure 2 is presented in figure 3, which shows the phase portrait of integer order of system (1) for a specific value of a.

From figure 3a, we notice that integer order of system (1) displays bistable double-scroll chaotic attractors with the same shape and parameter value but with different initial conditions. The bistable double-scroll chaotic attractors of figure 3a merge to give four-scroll chaotic attractors as illustrated in figure 3b. The shapes of bistable double-scroll chaotic attractors and four-scroll chaotic attractors in figure 3 are different from those found in [41]. The phase portraits of the coexisting attractors of integer order of system (1) are shown in figures 4a, 4b, 4c1 and 4c2 for $a = 3.53$ and for specific initial conditions.

At $a = 3.53$, the integer-order system (1) displays four-scroll chaotic attractor, a pair of double-scroll chaotic attractors and a pair of point attractors for each starting point $(x(0), y(0), z(0))$, as illustrated in the caption of figure 4.

2.2 *Analysis of the fractional-order three-dimensional autonomous system with hyperbolic sine nonlinearity*

In this subsection, the effect of fractional derivation in system (1) is investigated for specific values of a. For $a = 3.53$, numerical simulations reveal that when $0.98 \leq q < 1$, the commensurate fractional order of system (1) exhibits a coexistence of attractors between a pair of double-scroll chaotic attractors and a pair of point attractors. These coexisting attractors are illustrated in figures 5a, 5b1 and 5b2 for commensurate fractional order $q = 0.98$.

At $q = 0.98$, the long-term behaviour of the commensurate fractional order of system (1) is a pair of double-scroll chaotic attractors and a pair of point attractors for each starting point $(x(0), y(0), z(0))$, as illustrated in figure 5. For $a = 3.53$ and $q < 0.95$, the trajectories of commensurate fractional order of system (1) converge either to the equilibrium point E_2 or E_4.

For $a = 3.35$, to know the effect of commensurate fractional order on four-scroll chaotic attractors found in figure 3b, we plot in figures 6a, 6b, 6c1 and 6c2 the phase portraits of commensurate fractional order of system (1) for some discrete values of commensurate fractional order q.

In figure 6, by decreasing the commensurate fractional order, the commensurate fractional order of system (1) exhibits four-scroll chaotic attractor, a pair of double-scroll chaotic attractors and a pair of point attractors.

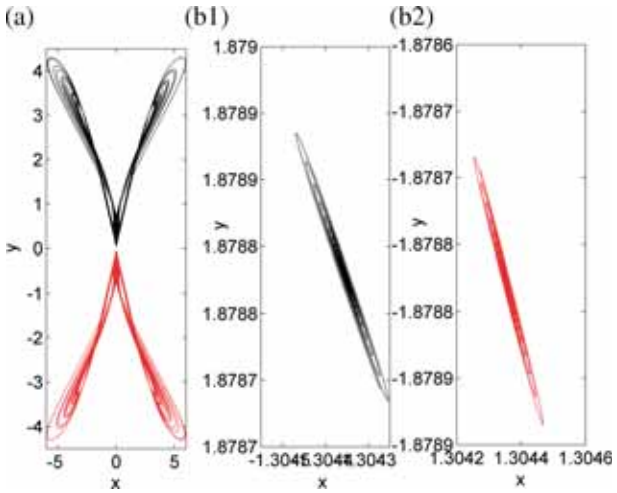

Figure 5. Phase portraits in the (x, y) plane of coexisting attractors in commensurate fractional-order system (1) at $a = 3.53$, $q = 0.98$ and for specific values of the starting points: (**a**) $(x(0), y(0), z(0)) = (0.1, 0.1, 0.1)$ for black line and $(x(0), y(0), z(0)) = (-0.1, -0.1, 0.1)$ for red line, (**b1**) $(x(0), y(0), z(0)) = (-1.3052, 1.8788, -2.4506)$ and (**b2**) $(x(0), y(0), z(0)) = (1.3052, -1.8788, -2.4506)$.

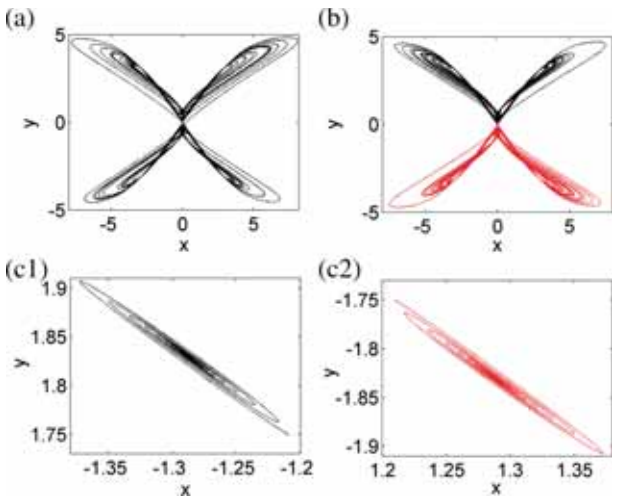

Figure 6. Phase portraits in the (x, y) plane in commensurate fractional order of system (1) with $a = 3.35$: (**a**) $q = 0.999$, (**b**) $q = 0.98$ and (**c1**) and (**c2**) $q = 0.96$. For black trajectory, the starting point is $(x(0), y(0), z(0)) = (0.1, 0.1, 0.1)$, whereas for the red trajectory, the starting point is $(x(0), y(0), z(0)) = (-0.1, -0.1, 0.1)$.

For $a = 1.5$, the integer order of system (1) exhibits four-scroll chaotic attractors [41]. Equation (6) illustrates the equilibrium points with their eigenvalues:

$$E_0(0, 0, 0) : \lambda_1 = -1.5,\ \lambda_{2,3} = \pm 1.0, \tag{6a}$$

$$E_{1,2}(\pm 1.126691522, 1.224744871, \pm 1.379909663) :$$

$$\lambda_1 = -6.971613,$$

$$\lambda_{2,3} = 0.3581724360 \pm 1.535190801\text{j}, \tag{6b}$$

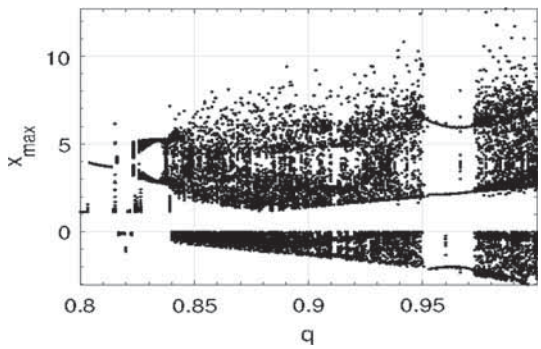

Figure 7. Bifurcation diagram showing the local maxima of the state variable $x(t)$, $x_{\max}$ with respect to the commensurate fractional-order q of system (1). The parameter is $a = 1.5$ and initial conditions are (0.1, 0.1, 0.1).

$$E_{3,4}(\pm 1.126691522, -1.224744871, \mp 1.379909663):$$

$$\lambda_1 = -6.971613,$$

$$\lambda_{2,3} = 0.3581724360 \pm 1.535190801\text{j}. \tag{6c}$$

Now, according to Tavazoei and Haeri [45], the equilibrium point E_0 is the saddle point of index 1, whereas equilibrium points $E_{1,2}$ and $E_{3,4}$ are the saddle points of index 2. Tavazoei and Haeri [45] provided the following inequality that can help to obtain stability criterion:

$$\arg(0.3581724360 \pm 1.535190801\text{j}) > \pi q/2$$
$$\Rightarrow q < 0.8540816583.$$

Therefore, the necessary condition for the commensurate fractional order of system (1) to behave chaotically is $q \geq 0.8540816583$. As the aforementioned condition is a necessary but not sufficient condition, it does not warrant chaos itself [45]. In order to find the smallest value of commensurate fractional-order q of system (1) to remain chaotic, we investigated numerically the effect of fractional derivation on the chaotic autonomous system with hyperbolic sine nonlinearity for the specific value of $a = 1.5$. Therefore, the bifurcation diagram illustrating the local maxima of the state variable $x(t)$, $x_{\max}$, is plotted vs. the fractional-order q as shown in figure 7.

In figure 7, when the commensurate fractional-order q varies from 0.8 to 1.0, the trajectories of system (1) converge to the equilibrium point $O = (0, 0, 0)$ up to $q = 0.805$, where a Hopf bifurcation occurs followed by period-1 oscillations up to $q = 0.839$ and chaos interspersed with periodic windows. The bifurcation diagram of figure 7 reveals that for $q \geq 0.839$, commensurate fractional order of system (1) is chaotic. Therefore, the smallest value of the commensurate fractional order of system (1) to exhibit chaos is $3q \approx 2.517$. We show in figure 8 the phase portraits of commensurate fractional order of system (1) in the planes (x, y), (y, z) and (x, z)

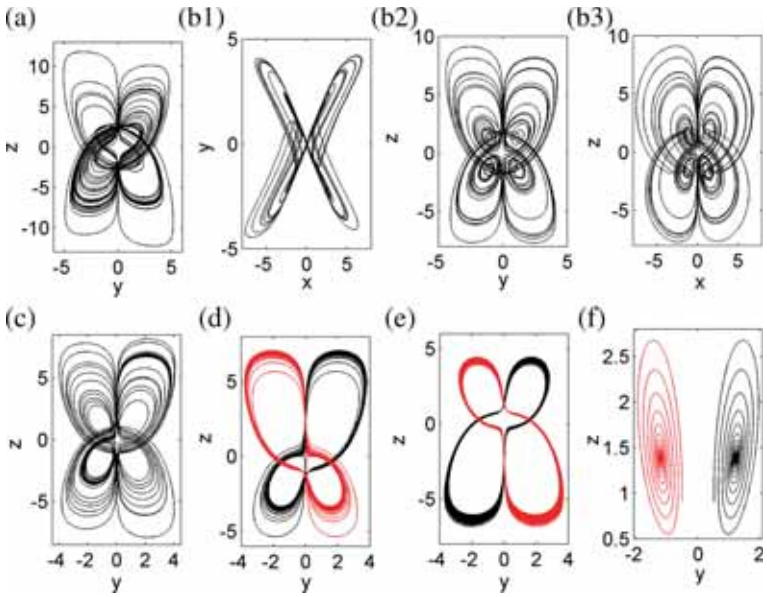

Figure 8. Phase portraits in the (x, y), (y, z) and (x, z) planes in commensurate fractional-order system (1) when $a = 1.5$ for specific values of commensurate fractional-order q: (**a**) $q = 0.98$, (**b**) $q = 0.9$, (**c**) $q = 0.84$, (**d**) $q = 0.839$, (**e**) $q = 0.827$ and (**f**) $q = 0.825$. The curve in black is obtained by using the initial conditions $(x(0), y(0), z(0)) = (0.1, 0.1, 0.1)$, whereas the curve in red is obtained by using the starting point $(x(0), y(0), z(0)) = (-0.1, -0.1, 0.1)$.

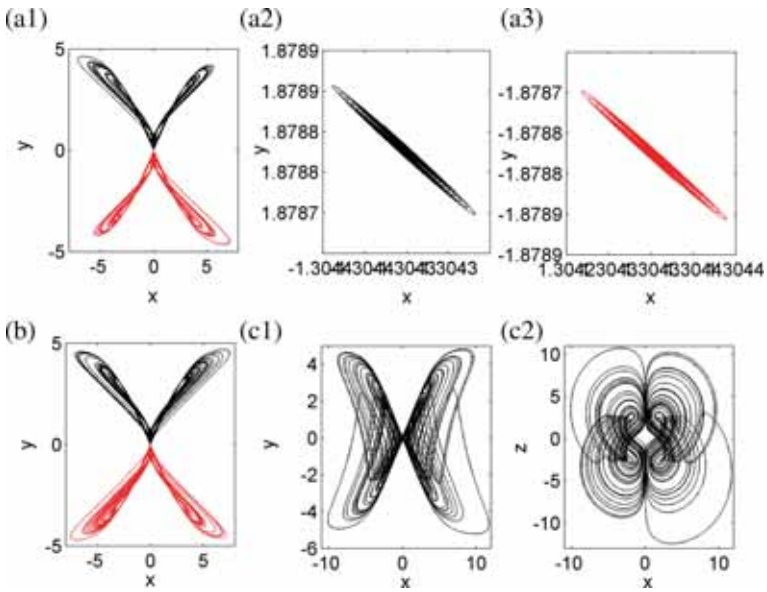

Figure 9. Phase portraits in the (x, y) and (x, z) planes of incommensurate fractional-order system (1) at $q_1 = 0.99$, $q_2 = 0.98$, $q_3 = 1.0$ and for specific values of the parameter a: (**a**) $a = 3.53$, (**b**) $a = 3.35$ and (**c**) $a = 1.5$. In (**a1**), (**b**), (**c1**) and (**c2**), curve in black is obtained by using the initial conditions $(x(0), y(0), z(0)) = (0.1, 0.1, 0.1)$, whereas the curve in red is obtained by using the initial conditions $(x(0), y(0), z(0)) = (-0.1, -0.1, 0.1)$. In (**a2**) and (**a3**), the starting points are $(x(0), y(0), z(0)) = (-1.3052, 1.8788, -2.4506)$ and $(x(0), y(0), z(0)) = (1.3052, -1.8788, -2.4506)$, respectively.

for some discrete values of commensurate fractional-order q.

Figure 8 reveals that commensurate fractional order of system (1) exhibits four-scroll chaotic attractor for $0.84 \leq q \leq 1.0$ (see figures 8a–8c), bistable double-scroll chaotic attractor for $q = 0.839$ (see figure 8d), bistable period-1 oscillations for $0.827 \leq q < 0.839$ (see figure 8e) and bistable point attractor for $q \leq 0.826$ (see figure 8f). Phase portraits plotted in figures 9a1, 9a2, 9a3, 9b, 9c1 and 9c2 confirm

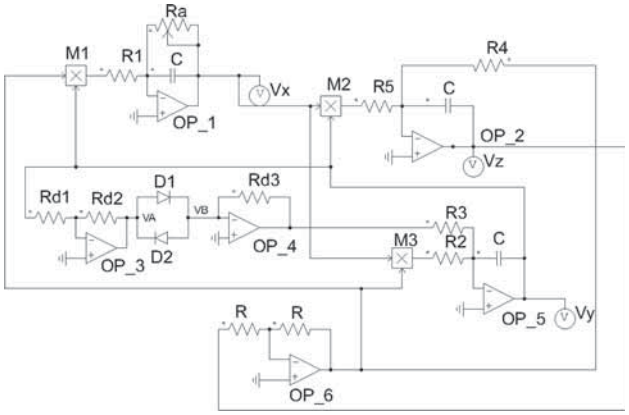

Figure 10. Circuit of integer order of system (1).

that bistable double-scroll chaotic attractors, four-scroll chaotic attractors and coexistence of attractors between a pair of double-wing chaotic attractors and a pair of point attractors exist in the incommensurate fractional order of system (1) as well.

3. Electronic circuit simulations of integer- and fractional-order three-dimensional autonomous systems with hyperbolic sine nonlinearity

In this section, using PSIM software, electronic circuits of integer order and commensurate fractional order of system (1) are proposed with the objective of verifying the results found in §2.2.

3.1 *Circuit implementation of integer-order three-dimensional autonomous system with hyperbolic sine nonlinearity*

The circuit implementation of the integer order of system (1) is shown in figure 10.

The circuit of figure 10 is made of 10 resistors with fixed values and one resistor with a variable value, three ceramic capacitors C of 10 nF, six TL082 operational amplifiers (OP_1 to OP_6), three AD633JN multiplier chips (M1 to M3) and two antiparallel 1N4148 diodes (D1 and D2). The quadratic terms are built using three multiplier chips (AD633JN) of gain 1 V^{-1}, whereas the hyperbolic sine nonlinearity function is implemented using two diodes in antiparallel direction. The current flow in the two diodes in antiparallel direction is given by

$$i_{\mathrm{D}} = I_s\left\{\mathrm{e}^{\frac{V_{\mathrm{AB}}}{\eta V_t}} - \mathrm{e}^{-\frac{V_{\mathrm{AB}}}{\eta V_t}}\right\} = 2I_s \sinh\left[\frac{V_{\mathrm{AB}}}{\eta V_t}\right],$$

where I_{s} is the reversed bias current, η is the ideal diode factor and V_{t} is the thermal voltage. Applying Kirchhoff's laws to the circuit of figure 10, we obtain the following three first-order differential equations:

$$C\frac{\mathrm{d}V_x}{\mathrm{d}t'} = -\frac{V_x}{R_a} + \left(\frac{V_y V_z}{1V}\right)\frac{1}{R_1}, \tag{7a}$$

$$C\frac{\mathrm{d}V_y}{\mathrm{d}t'} = \left(\frac{V_x V_z}{1V}\right)\frac{1}{R_2} - 2I_s\frac{R_{\mathrm{d3}}}{R_3}\sinh\left(\frac{R_{\mathrm{d1}}V_y}{R_{\mathrm{d2}}\eta V_t}\right), \tag{7b}$$

$$C\frac{\mathrm{d}V_z}{\mathrm{d}t'} = \frac{V_z}{R_4} - \left(\frac{V_x V_y}{1V}\right)\frac{1}{R_3}. \tag{7c}$$

We rescaled system (7) by introducing the timeless variable $t = (t'/RC)$. System (8) is written as follows:

$$\frac{\mathrm{d}X}{\mathrm{d}t} = -\frac{R}{R_a}X + \frac{R}{R_1}YZ, \tag{8a}$$

$$\frac{\mathrm{d}Y}{\mathrm{d}t} = \frac{R}{R_2}XZ - 2R\frac{R_{\mathrm{d3}}}{R_3}I_s\sinh\left(\frac{R_{\mathrm{d1}}V_y}{R_{\mathrm{d2}}\eta V_t}\right), \tag{8b}$$

$$\frac{\mathrm{d}Z}{\mathrm{d}t} = \frac{R}{R_4}Z - \frac{R}{R_3}XY. \tag{8c}$$

For system (8) to be equivalent to the integer order of system (1), we set the following values to the parameters: $R = R_1 = R_2 = R_3 = R_4 = 30\,\mathrm{k\Omega}$, $R_{\mathrm{d2}} = 2.5\,\mathrm{k\Omega}$, $R_{\mathrm{d3}} = 186.5\,\mathrm{M\Omega}$, $\mathrm{Ra} = R/a$, $R_{\mathrm{d1}} = \eta V_t R_{\mathrm{d2}} = 100\,\mathrm{k\Omega}$ and $R_3 = 2RI_sR_{\mathrm{d3}} = 0.1119\,\Omega$, where X stands for V_x, Y for V_y and Z for V_z. Figures 11a, 11b and 12a, 12b, 12c1 and 12c2 and present the phase portraits of integer order of system (1) obtained from the design circuit of figure 10 for specific values of knob resistor Ra.

Figures 11 and 12 show that the numerical results (figures 3 and 4, respectively) and analogue results are in good agreement.

3.2 *Circuit implementation of commensurate fractional-order three-dimensional autonomous system with hyperbolic sine nonlinearity*

The circuit implementation of commensurate fractional-order chaotic three-dimensional autonomous system with the nonlinearity function $f(x) = \sinh(x)$ for $q = 0.9$ is obtained by substituting the capacitors C in figure 10 by three fractance elements shown in figure 13.

Figure 14 presents the phase portraits of commensurate fractional order of system (1) obtained from the design circuit for specific value of resistor Ra.

Phase portraits of figure 14 obtained in PSIM software are in good agreement with phase portraits in

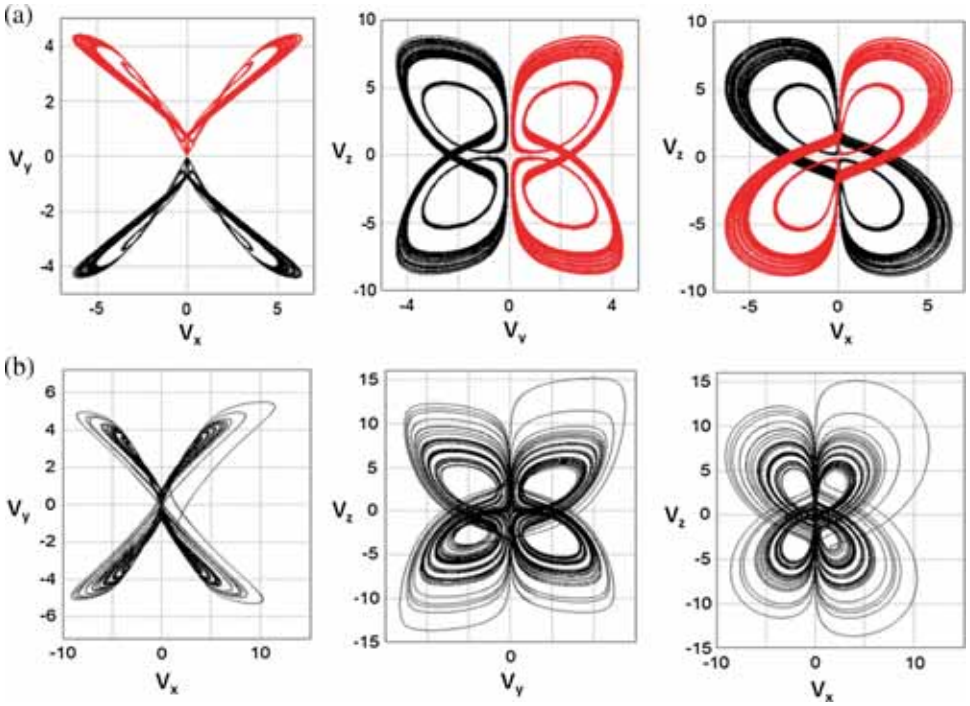

Figure 11. Phase portraits of the designed circuit obtained by using PSIM analogue simulator in (V_x, V_y), (V_y, V_z) and (V_x, V_z) planes for critical values of the knob resistor Ra: (**a**) Ra = 8.44 kΩ and (**b**) Ra = 8.45 kΩ. The curves in black is obtained by using the initial capacitor voltages ($Vx(0) = 0.1$ V, $Vy(0) = 0.1$ V, $Vz(0) = 0.1$ V), whereas the curves in red are obtained by using the initial capacitor voltages ($Vx(0) = -0.1$ V, $Vy(0) = 0.1$ V, $Vz(0) = 0.1$ V).

figures 8b1–8b3. Hence, the fractional order of the studied circuit is successfully implemented using the fractance elements.

4. Combination synchronisation of commensurate fractional-order chaotic three-dimensional autonomous system with hyperbolic sine nonlinearity

The synchronisation of a one-drive chaotic system with a response system may have possible potential applications in secure communication because chaotic signals are difficult to predict [49,50]. However, this kind of communication system is relatively easier to be attacked or decoded because there is only one transmitter. Hence, splitting the original information into two or more parts and embedding different parts in different drive systems can help in enormously enhancing the anti-attack and anti-decode ability [51–53]. This type of synchronisation between two or more drive systems and one response system is referred to as combination synchronisation [51–53]. The aim of this section is to study the combination synchronisation of two drive commensurate fractional order of system (1) and one response commensurate fractional order of system (1) using

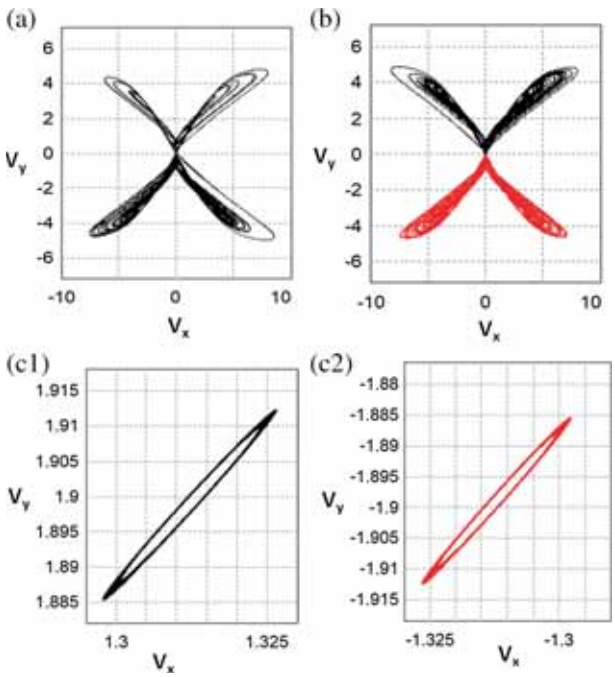

Figure 12. Phase portraits of the designed circuit in figure 10 obtained by using PSIM analogue simulator in the (V_x, V_y) plane for specific initial capacitor voltages ($Vx(0)$, $Vy(0)$, $Vz(0)$): (**a**) (−1.3052 V, −0.1 V, −2.4506 V), (**b**) (2 V, 0.1 V, 0.1 V) for black line and (−2 V, 0.1 V, 0.1 V) for red line, (**c1**) (−1.3052 V, −2.4506 V, −1.8788 V) and (**c2**) (−1.3052 V, −2.4506 V, 1.8788 V). The value of the knob resistor is Ra = 6.26 kΩ.

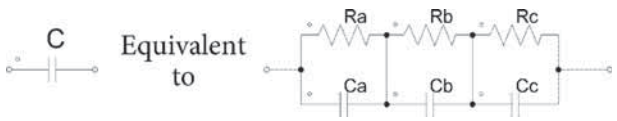

Figure 13. Ladder-type fractional elements of the capacitor C for $q = 0.9$: Ra $= 62.84\,\text{M}\Omega$, Rb $= 0.25\,\text{M}\Omega$, Rc $= 2.5\,\text{M}\Omega$, Ca $= 1.232\,\mu\text{F}$, Cb $= 1.84\,\mu\text{F}$ and Cc $= 1.1\,\mu\text{F}$. Initial voltages of the capacitors are $V_{\text{Ca}}(0) = V_{\text{Cb}}(0) = V_{\text{Cc}}(0) = 0.1\,\text{V}$. The computation values of the capacitors and resistors are explained in detail in [46–48].

active backstepping design. The drive–response commensurate fractional order of system (1) is expressed as

$$\frac{\mathrm{d}^q x_m}{\mathrm{d}t^q} = -a x_m + y_m z_m, \tag{9a}$$

$$\frac{\mathrm{d}^q y_m}{\mathrm{d}t^q} = x_m z_m - \sinh(y_m), \tag{9b}$$

$$\frac{\mathrm{d}^q z_m}{\mathrm{d}t^q} = z_m - x_m y_m, \tag{9c}$$

where $m = 1, 2$ and

$$\frac{\mathrm{d}^q x_s}{\mathrm{d}t^q} = -a x_s + y_s z_s + u_1, \tag{10a}$$

$$\frac{\mathrm{d}^q y_s}{\mathrm{d}t^q} = x_s z_s - \sinh(y_s) + u_2, \tag{10b}$$

$$\frac{\mathrm{d}^q z_s}{\mathrm{d}t^q} = z_s - x_s y_s + u_3, \tag{10c}$$

where u_i $(i = 1, 2, 3)$ are the controllers to be designed such that the three systems can be synchronised. For this purpose, let the state errors be $e = Ax + By - Cz$, where

$$x = (x_1, y_1, z_1)^{\mathrm{T}}, \quad y = (x_2, y_2, z_2)^{\mathrm{T}},$$
$$z = (x_s, y_s, z_s)^{\mathrm{T}}, \quad e = (e_x, e_y, e_z)^{\mathrm{T}},$$

and $A, B, C \in R^{3\times 3}$. Choose some suitable control functions u_i $(i = 1, 2, 3)$, such that $\lim_{t\to\infty} \|Ax + By - Cz\| = 0$. Then the three systems will approach synchronisation. For the convenience of our discussions, we assume that $A = \text{diag}(\eta_1, \eta_2, \eta_3)$, $B = \text{diag}(\gamma_1, \gamma_2, \gamma_3)$ and $C = \text{diag}(\varepsilon_1, \varepsilon_2, \varepsilon_3)$, and then we get the error dynamical system as follows:

$$e_x = \eta_1 x_1 + \gamma_1 x_2 - \varepsilon_1 x_s, \tag{11a}$$

$$e_y = \eta_2 y_1 + \gamma_2 y_2 - \varepsilon_2 y_s, \tag{11b}$$

$$e_x = \eta_3 z_1 + \gamma_3 z_2 - \varepsilon_3 z_s. \tag{11c}$$

It is easy to see from the set of eq. (11) that the error dynamical system can be obtained as follows:

$$\frac{\mathrm{d}^q e_x}{\mathrm{d}t^q} = \eta_1 \frac{\mathrm{d}^q x_1}{\mathrm{d}t^q} + \gamma_1 \frac{\mathrm{d}^q x_2}{\mathrm{d}t^q} - \varepsilon_1 \frac{\mathrm{d}^q x_s}{\mathrm{d}t^q}, \tag{12a}$$

$$\frac{\mathrm{d}^q e_y}{\mathrm{d}t^q} = \eta_2 \frac{\mathrm{d}^q y_1}{\mathrm{d}t^q} + \gamma_2 \frac{\mathrm{d}^q y_2}{\mathrm{d}t^q} - \varepsilon_2 \frac{\mathrm{d}^q y_s}{\mathrm{d}t^q}, \tag{12b}$$

$$\frac{\mathrm{d}^q e_z}{\mathrm{d}t^q} = \eta_3 \frac{\mathrm{d}^q z_1}{\mathrm{d}t^q} + \gamma_3 \frac{\mathrm{d}^q z_2}{\mathrm{d}t^q} - \varepsilon_3 \frac{\mathrm{d}^q z_s}{\mathrm{d}t^q}. \tag{12c}$$

Substituting eqs (9)–(11) into eqs (12a)–(12c), we get

$$\frac{\mathrm{d}^q e_x}{\mathrm{d}t^q} = -a e_x + \eta_1 y_1 z_1 + \gamma_1 y_2 z_2 - \varepsilon_1 y_s z_s - \varepsilon_1 u_1, \tag{13a}$$

$$\frac{\mathrm{d}^q e_y}{\mathrm{d}t^q} = \eta_2 x_1 z_1 - \eta_2 \sinh(y_1) + \gamma_2 x_2 z_2 - \gamma_2 \sinh(y_2) - \varepsilon_2 z_s + \varepsilon_2 \sinh(y_s) - \varepsilon_2 u_2, \tag{13b}$$

$$\frac{\mathrm{d}^q e_z}{\mathrm{d}t^q} = e_z - \eta_3 x_1 y_1 - \gamma_3 x_2 y_2 + \varepsilon_3 x_s y_s - \varepsilon_3 u_3. \tag{13c}$$

The controller laws are chosen as follows:

$$u_1 = (\eta_1 y_1 z_1 + a\gamma_1 y_2 z_2 - \varepsilon_1 y_s z_s - v_1)/\varepsilon_1, \tag{14a}$$

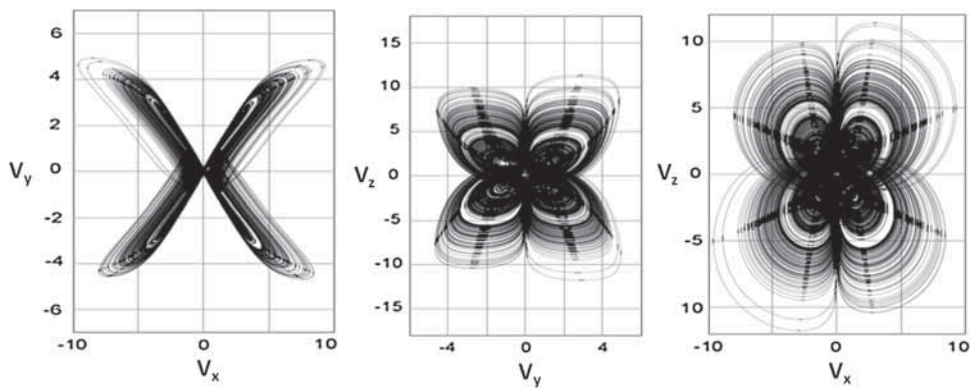

Figure 14. PSIM phase portraits of four-wing chaotic attractor in (V_x, V_y), (V_y, V_z) and (V_x, V_z) planes for $q = 0.9$. The value of resistance is Ra $= 19.8\,\text{k}\Omega$. The rest of the component values are the same as in the caption of figure 10. Initial voltage of capacitors is 0.1 V.

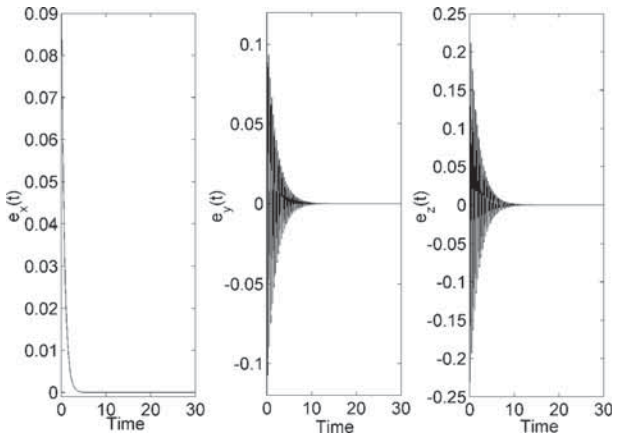

Figure 15. Synchronisation errors for $a = 1.5$, $q = 0.9$ and the control parameters $\eta_1 = \eta_2 = \eta_3 = 1, \gamma_1 = \gamma_2 = \gamma_3 = 1$, $\varepsilon_1 = \varepsilon_2 = \varepsilon_3 = 0.5$.

$$u_2 = (\eta_2 x_1 z_1 - \eta_2 \sinh(y_1) + \gamma_2 x_2 z_2 - \gamma_2 \sinh(y_2) - \beta\varepsilon_2 x_s z_s + \sinh(y_s) - v_2)/\varepsilon_2, \quad (14b)$$

$$u_3 = [-\eta_3 x_1 y_1 - \gamma_3 x_2 y_2 + \varepsilon_3 x_s y_s - v_3]/\varepsilon_3, \quad (14c)$$

where v_i are chosen by suitable linear functions of the error terms e_i $(i = x, y, z)$, and we choose it such that the error dynamics becomes stable. The general form of such functions is

$$\begin{pmatrix} v_x \\ v_y \\ v_z \end{pmatrix} = \bar{A} \begin{pmatrix} e_x \\ e_y \\ e_z \end{pmatrix}, \quad (15)$$

where

$$A = \begin{pmatrix} a_{11} & a_{12} & a_{13} \\ a_{21} & a_{22} & a_{23} \\ a_{31} & a_{32} & a_{33} \end{pmatrix}$$

is a 3×3 real matrix. The condition $|\arg(\lambda_i)| > q\pi/2$ is satisfied when λ_i are the eigenvalues of the error dynamical system. If we choose $a_{11} = 0$, $a_{12} = 0$, $a_{13} = 0$, $a_{21} = 0$, $a_{22} = 0$, $a_{23} = 8.5$, $a_{31} = -1.5$, $a_{32} = -38$, $a_{33} = -2$, then the error dynamical system is

$$\frac{\mathrm{d}^q e_x}{\mathrm{d}t^q} = -1.5 e_x, \quad (16a)$$

$$\frac{\mathrm{d}^q e_y}{\mathrm{d}t^q} = 8.5 e_z, \quad (16b)$$

$$\frac{\mathrm{d}^q e_z}{\mathrm{d}t^q} = -1.5 e_x - 38 e_y - e_z. \quad (16c)$$

As $a = 1.5$ and $q = 0.9$, we get three eigenvalues $\lambda_1 = -1.5, \lambda_2 = -0.5 + 17.96524422\mathrm{j}$ and $\lambda_3 = -0.5 - 17.96524422\mathrm{j}$, which satisfy $|\arg(\lambda_i)| = 1.542971992 = 0.45\pi$. This ensures that the error states asymptotically converge to zero as $t \to \infty$, and therefore, the combination synchronisation between the drive–response systems (9) and (10) is achieved. For the purpose of numerical simulations, we set $a = 1.5$ and $q = 0.98$ with the initial conditions of the drive and response systems (9) and (10): $(x_1(0), y_1(0), z_1(0)) = (0.1, 0.1, 0.1)$, $(x_2(0), y_2(0), z_2(0)) = (2, -0.1, 0.1)$ and $(x_s(0), y_s(0), z_s(0)) = (2, -0.1, 0.1)$ to ensure four-scroll chaotic attractors. In figure 15, the synchronisation errors between the drive and the response systems (9) and (10) are plotted in order to check the effectiveness of the design controllers.

Figure 15 shows that the asymptotical convergence of the synchronisation errors decay to zero. As shown in the numerical simulations, the design controllers can synchronise the drive and the response systems (9) and (10).

5. Conclusion

This paper deals with the analysis and combination synchronisation of integer- and fractional-order chaotic systems with hyperbolic sine nonlinearity. Thanks to the Routh–Hurwitz criterion and linear stability of the equilibrium points, it was found that transcritical bifurcation occurs in integer-order chaotic system with the nonlinearity function $f(x) = \sinh(x)$. The numerical results indicate that integer- and fractional-order chaotic systems with hyperbolic sine nonlinearity exhibit new complex shapes of bistable double-scroll chaotic attractors and four-scroll chaotic attractors and coexistence of attractors. The designed circuits were implemented and tested using PSIM software to verify the numerical simulation results. Comparison of the PSIM and numerical simulation results showed good qualitative agreement between the integer-order and commensurate fractional-order chaotic systems with hyperbolic sine nonlinearity and their circuitry implementations. To the best of our knowledge, the results obtained in this work (the illustration and the physical proof of existence of multiwing coexisting attractors found in the integer-order and commensurate fractional order of the systems with hyperbolic sine nonlinearity) have not been reported previously in three-dimensional autonomous systems with hyperbolic sine nonlinearity and thus represent an enriching contribution to the understanding of the dynamics of this class of systems. Finally, conditions for achieving combination synchronisation between drive–response commensurate fractional-order chaotic systems with hyperbolic sine nonlinearity were presented and numerical simulations were carried out to check the analytical investigation.

References

[1] E N Lorenz, *J. Atmos. Sci.* **20**, 130 (1963)
[2] S H Strogatz, *Nonlinear dynamics and chaos: With applications to physics, biology, chemistry, and engineering* (Westview Press, Massachusetts, 2014)
[3] M Lakshmanan and D V Senthilkumar, *Dynamics of nonlinear time-delay systems* (Springer Science & Business Media, Heidelberg, 2011)
[4] A Buscarino, L Fortuna, M Frasca and L V Gambuzza, *Int. J. Bifurc. Chaos* **23**, 1330015 (2013)
[5] S Jafari, S Dehghan, G Chen, S T Kingni and K Rajagopal, *Chaos Solitons Fractals* **112**, 135 (2018)
[6] P S Shabestari, S Panahi, B Hatef, S Jafari and J C Sprott, *Chaos Solitons Fractals* **112**, 44 (2018)
[7] Z Wei, A Akgul, U E Kocamaz, I Moroz and W Zhang, *Chaos Solitons Fractals* **112**, 157 (2018)
[8] P Zhou, R Bai and J Zheng, *Nonlinear Dyn.* **82**, 519 (2015)
[9] J Ma, Q Y Wang, W Y Jin and Y F Xia, *Chin. Phys. Lett.* **25**, 3582 (2008)
[10] J C Sprott, *Elegant chaos: Algebraically simple flow* (World Scientific Publishing, Singapore, 2010)
[11] I Petras, *Fractional-order nonlinear systems: Modeling, analysis and simulation* (Springer, China, 2011)
[12] P Zhou and P Zhu, *Nonlinear Dyn.* **89**, 1719 (2017)
[13] Q Yin and C Wang, *Int. J. Bifurc. Chaos* **28**, 1850047 (2018)
[14] L Zhou, C Wang, X Zhang and W Yao, *Int. J. Bifurc. Chaos* **28**, 1850050 (2018)
[15] X Wang, A Akgul, S Cicek, V-T Pham and D V Hoang, *Int. J. Bifurc. Chaos* **27**, 1750130 (2017)
[16] A Kiani-B, K Fallahi, N Pariz and H Leung, *Commun. Nonlinear Sci. Numer. Simul.* **14**, 863 (2009)
[17] P Muthukumar and P Balasubramaniam, *Nonlinear Dyn.* **74**, 1169 (2013)
[18] A S Elwakil, S Özoguz and M P Kennedy, *Int. J. Bifurc. Chaos* **13**, 3093 (2003)
[19] G Qi, G Chen, M A Wyk, B J Wyk and Y Zhang, *Chaos Solitons Fractals* **38**, 705 (2008)
[20] Q Lai, Z H Guan, Y Wu, F Liu and D X Zhang, *Int. J. Bifurc. Chaos* **23**, 1350152 (2013)
[21] S Yu, W K S Tang, J Lü and G Chen, *Int. J. Bifurc. Chaos* **20**, 29 (2010)
[22] C Zhang and S Yu, *Int. J. Circuit Theory Appl.* **41**, 221 (2013)
[23] S Yu, J Lü, G Chen and X Yu, *IEEE Trans. Circuit Syst. I: Regul. Pap.* **59**, 1015 (2012)
[24] N Yu, Y W Wang, X K Liu and J W Xiao, *Int. J. Bifurc. Chaos* **28**, 1850045 (2018)
[25] H Jia, Z Guo, Q Qi and Z Chen, *Optik* **155**, 233 (2018)
[26] J H Lü and G R Chen, *Int. J. Bifurc. Chaos* **16**, 775 (2006)
[27] A N Pisarchik and U Feudel, *Phys. Rep.* **540**, 167 (2014)
[28] X Luo and M Small, *Int. J. Bifurc. Chaos* **17**, 3235 (2007)
[29] C Hens, S K Dana and U Feudel, *Chaos: Interdiscip. J. Nonlinear Sci.* **25**, 053112 (2015)
[30] B C Bao, B Xu, H Bao and M Chen, *Electron. Lett.* **52**, 1008 (2016)
[31] B Bao, T Jiang, Q Xu, M Chen, H Wu and Y Hu, *Nonlinear Dyn.* **86**, 1711 (2016)
[32] J Kengne, Z T Njitacke and H B Fotsin, *Nonlinear Dyn.* **83**, 751 (2016)
[33] J Kengne, A Nguomkam Negou and Z T Njitacke, *Int. J. Bifurc. Chaos* **27**, 1750100 (2017)
[34] A Massoudi, M G Mahjani and M Jafarian, *J. Electroanal. Chem.* **647**, 74 (2010)
[35] Z T Njitacke, J Kengne and L Kamdjeu Kengne, *Chaos Solitons Fractals* **105**, 77 (2017)
[36] J Kengne, A Nguomkam Negou and D Tchiotsop, *Nonlinear Dyn.* **88**, 2589 (2017)
[37] A Nguomkam Negou, J Kengne and D Tchiotsop, *Chaos Solitons Fractals* **107**, 275 (2018)
[38] V-T Pham, C Volos, S T Kingni, S Jafari and T Kapitaniak, *Nonlinear Dyn.* **87**, 2001 (2017)
[39] J P Singh, K Rajagopal and B K Roy, *Pramana – J. Phys.* **91**, 33 (2018)
[40] X Xia, Y Zeng and Z Li, *Pramana – J. Phys.* **91**: 82 (2018)
[41] Z Wang, C K Volos, S T Kingni, A Taher Azar and V-T Pham, *Optik* **131**, 1071 (2017)
[42] R Caponetto, R Dongola, L Fortuna and I Petras, *World Sci. Ser. Nonlinear Sci. A* **72**, 200 (2010)
[43] R Hilfer, *Applications of fractional calculus in physics* (World Scientific, New Jersey, 2001)
[44] K Diethelm, N J Ford and D Freed, *Nonlinear Dyn.* **29**, 3 (2002)
[45] M S Tavazoei and M Haeri, *Phys. Lett. A* **367**, 102 (2007)
[46] G E Carlson and C A Halijak, *IEEE Trans. Circuit Theory* **11**, 210 (1964)
[47] S Westerlund and L Ekstam, *IEEE Trans. Dielectr. Electr. Insul.* **1**, 826 (1994)
[48] S-P Wang, S-K Lao, H-K Chen, J-H Chen and S-Y Chen, *Int. J. Bifurc. Chaos* **23**, 1350030 (2013)
[49] B Nana, P Woafo and S Domngang, *Commun. Nonlinear Sci. Numer. Simul.* **14**, 2266 (2009)
[50] N Smaoui, A Karouma and M Zribi, *Commun. Nonlinear Sci. Numer. Simul.* **16**, 3279 (2011)
[51] R Z Luo, Y L Wang and S C Deng, *Chaos* **21**, 043114 (2011)
[52] R Z Luo and Y L Wang, *Chaos* **22**, 023109 (2012)
[53] Z Alam, L Yuan and Q Yang, *J. Autom. Sin.* **3**, 157 (2016)